Optimization of the micro-textures on the cutting tool based on the penetration of the lubricant in the micro-textures

Xin Liu[1] · Yu Liu[1] · Lei Li[1] · Yuan Tian[2]

Abstract

In recent years, surface textures in micron scale is introduced into the rake face of cutting tools to facilitate the lubricant penetration into the cutting area and improving the friction conditions between tool-chip contact area. The penetration process of lubricant into micro-textures introduced into the rake face of the cutting tool during machining process is analyzed through theory calculation, FEA analysis and penetration experiments. It is found that the initial penetration velocity increases as the size of the micro-texture decreases; However, due to the combined effect of capillary pressure and friction force, the penetration distance for micro-texture with larger size is longer than that for micro-texture with smaller size when the penetration distance is larger than 0.15 mm; micro-texture with smaller size is suitable for smaller chip width, 0.15 mm under the conditions in this study, and micro-texture with a larger size is more effective for large back engagement in consideration of lubricant penetration. Also, an optimum size of micro-texture on the rake face of cutting tools should take both lubricant penetration and strength of the cutting tool into consideration. The results of this study would benefit for the designation of micro-textures in the future.

Keywords Micro-texture · Cutting tool · Lubricant penetration · Optimization

1 Introduction

High-speed machining or even ultra-high-speed machining attracts many researchers attention due to the advantages of high-speed machining, such as high productive efficiency, small cutting force, high processing quality and low unit cutting power [1]. Inevitably, high cutting speed introduces high cutting temperature, and high pressure/high friction in the tool-chip contacting zone, which will cause fast tool wear during the cutting process. In order to overcome the disadvantages and extend the tool life during high-speed machining, lubricant is used to lower the cutting temperature and reduce the friction between the cutting tool and the workpiece material in industry applications [2, 3].

Studies earlier revealed that the penetration of the lubricant into the cutting zone occurred mainly by capillary action through microscopic passages existing between the tool-chip interface [4, 5]. However, these microscopic passages are not stable and would disappear in a very short time, which would not be long enough for the penetration of lubricant into the cutting zone. Hence, the cutting fluid is difficult to enter the cutting area and form effective lubricating film in the high-speed cutting process [6, 7]. The cooling and lubricating effect of the lubricant is then greatly reduced.

In order to solve this problem, micro-texture is introduced into the rake/flank face of the cutting tool to facilitate the penetration of cutting fluids and improve the friction conditions between tool-chip contact interface in recent years [8–24]. Researches show that on one hand micro-textures can enhance the ability of cutting fluids to penetrate the cutting zone, and on the other hand micro-textures can act as lubricant reservoirs, so that the lubricant can be fed into the cutting zone directly and form stable boundary lubrication layer. Fang et al. [25] fabricated five types of micro-textures on the flank face and proved that micro-textures could improve the cooling performance under the condition of high-pressure jet coolant assistance and this investigation clearly showed the function of micro-textures for increasing the

✉ Xin Liu
liu_xin2006@jlu.edu.cn

1   School of Mechanical and Aerospace Engineering, Jilin University, Changchun 130025, People's Republic of China

2   Changchun Vocational Institute of Technology, Changchun 130025, People's Republic of China

turbulent kinetic energy and cooling the textured tool face. Furthermore, Durairaj et al. [26] demonstrated that the lubrication enhancement of textured cutting tool would contribute to the effect that microscopic textures would act as a lubricant reservoir which is reached through capillary action. Moreover, Fatima et al. [27] fabricated a nature-inspired design (shape) of structure on the flank face of the cutting tool, and found out that the topography of the cutting tool face affects the quality of lubrication and thus the cutting temperature.

However, with the abundant existing works done, there are limitations when designing micro-textures with proper parameters learning from their work. Most researchers focused either on the mechanisms of the lubricant penetrating into the cutting zone and forming lubricating film, or on the turning experiments using micro-textured cutting tool to verify the effect of micro-textures on reducing adhesion, lowering cutting forces and cutting temperature and prolonging tool life. Optimization for the parameters of micro-textures is seldomly reported, especially the optimization of micro-textures based on the penetration ability of the lubricant.

In this study, the penetration process of lubricant into micro-textures on the rake face of the cutting tool during machining process is analyzed through theoretical calculation, FEA analysis and penetration experiments. The initial penetration velocity and penetration distance for micro-textures with different sizes are discussed at the same time. Optimization suggestion on the scale of the micro-textures is given based on the analysis results.

2 Theory calculation

During machining process, the tight contact between cutting chip and the tool rake face leads to poor penetration of lubricant into the cutting zone. Godlevski et al. concluded that the lubrication action works mainly by the penetration of the cutting lubricant into the tool-chip boundary through a dynamic network of interface capillaries [28]. However, the existing time of single capillary may not be long enough for the penetration of lubricant into the cutting zone. To prolong the penetration time of the lubricant and improve the lubrication conditions, micro-textures are introduced into the rake face of the cutting tool. Figure 1 shows the schematic of lubricant's penetration into micro-textures. The calculation of the initial penetration velocity of lubricant into the micro-textures is conducted on the premise of the following:

(1) The cutting chip and the rake face of the cutting tool is in tight contact;
(2) There is no additional pressure applied on the lubricant at the beginning of the penetration;
(3) The cross section of the micro-textures introduced into the rake face of the cutting tool is a circular shape.

Conclusions for different cross sections can be deduced by replacing the hydraulic radius in the final formula. And the micro-textures are open for both ends.

(4) The effect of cutting temperature, which would evaporate the lubricant, is neglected. Only liquid penetration state is considered.

For the incompressible Newtonian fluid with constant viscosity, the N-S equation in cylindrical coordinates can be written as:

$$
\left.
\begin{aligned}
&\rho \frac{\partial u_r}{\partial t} + \rho u_r \frac{\partial u_r}{\partial r} + \rho \frac{u_\theta}{r}\frac{\partial u_r}{\partial \theta} - \rho \frac{u_\theta^2}{r} + \rho u_z \frac{\partial u_r}{\partial z} \\
&\quad = -\frac{\partial p}{\partial r} + \mu \frac{\partial}{\partial r}\left[\frac{1}{r}\frac{\partial}{\partial r}(ru_r)\right] + \mu \frac{1}{r^2}\frac{\partial^2 u_r}{\partial \theta^2} - \mu \frac{2}{r^2}\frac{\partial u_\theta}{\partial \theta} + \mu \frac{\partial^2 u_r}{\partial z^2} + \rho g_r \\
&\rho \frac{\partial u_\theta}{\partial t} + \rho u_r \frac{\partial u_\theta}{\partial r} + \rho \frac{u_\theta}{r}\frac{\partial u_\theta}{\partial \theta} + \rho \frac{u_r u_\theta}{r} + \rho u_z \frac{\partial u_\theta}{\partial z} \\
&\quad = -\frac{1}{r}\frac{\partial p}{\partial \theta} + \mu \frac{\partial}{\partial r}\left[\frac{1}{r}\frac{\partial}{\partial r}(ru_\theta)\right] + \mu \frac{1}{r^2}\frac{\partial^2 u_\theta}{\partial \theta^2} + \mu \frac{2}{r^2}\frac{\partial u_r}{\partial \theta} + \mu \frac{\partial^2 u_\theta}{\partial z^2} + \rho g_\theta \\
&\rho \frac{\partial u_z}{\partial t} + \rho u_r \frac{\partial u_z}{\partial r} + \rho \frac{u_\theta}{r}\frac{\partial u_z}{\partial \theta} + \rho u_z \frac{\partial u_z}{\partial z} \\
&\quad = -\frac{\partial p}{\partial r} + \mu \frac{1}{r}\frac{\partial}{\partial r}\left(r\frac{\partial u_z}{\partial r}\right) + \mu \frac{1}{r^2}\frac{\partial^2 u_z}{\partial \theta^2} + \mu \frac{\partial^2 u_z}{\partial z^2} + \rho g_z
\end{aligned}
\right\}
$$

(1)

where:
ρ is the density of the lubricant;
r is the radius of the cross section of the micro-texture;
u_r, u_θ, and u_z are the radial, θ and z components of the velocity;
p is pressure on the lubricant;
and g represents the gravity of the lubricant.

Neglecting the effect of gravity due to the horizontal penetration of lubricant into the micro-texture, and simplifying the equation based on the symmetry of the lubricant penetration on x and y direction, the N-S equation can be shortened to:

$$
\left.
\begin{aligned}
&\frac{\partial v_l}{\partial t} + v_l \frac{\partial v_l}{\partial z} = \frac{1}{\rho}\frac{\partial p}{\partial z} + \frac{\nu}{\rho}\left(\frac{\partial^2 v_l}{\partial z^2} + \frac{1}{r}\frac{\partial v_l}{\partial r} + \frac{\partial^2 v_l}{\partial r^2}\right) \\
&\frac{\partial v_l}{\partial z} = 0
\end{aligned}
\right\}
$$

(2)

where:
$\frac{\partial v_l}{\partial z}$ represents the velocity gradient along the direction of the micro-texture;
$\frac{\partial p}{\partial z}$ is the pressure gradient.

Equation (2) describes the relationship of the initial penetration velocity v_l, kinematic viscosity v, time τ_l, pressure p, and the density ρ of the lubricant. By solving the equations, the initial penetration velocity v_l can be expressed as:

Fig. 1 a, b Schematic of lubricant's penetration into micro-textures

(a)

(b)
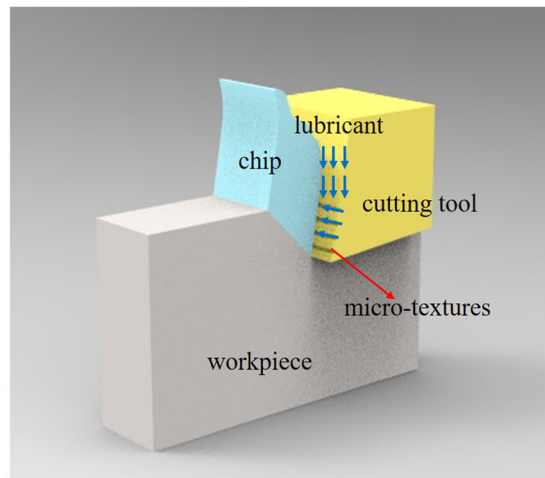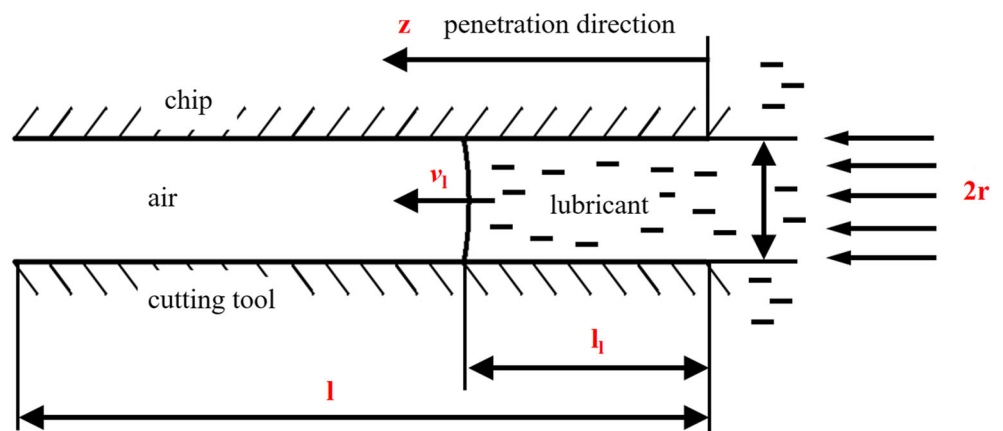
$$\frac{v_l}{\tau_l} \approx \frac{p}{\rho_l z} - \frac{\nu v_l}{\rho_l r^2} = \frac{p}{\rho_l v_l \tau_l} - \frac{\nu v_l}{\rho_l r^2} \quad (3)$$

where:

p the pressure on the lubricant, and $p = p_{atm} + \Delta p$;

p_{atm} means the pressure of the atmosphere and Δp is the pressure difference, which equals $\frac{2\sigma}{r}$;

σ is the surface tension coefficient.

The initial penetration velocity v_l can be obtained by solving Eq. (3):

$$v_l = \sqrt{\frac{p\chi}{\rho_l \chi + \nu}} = \sqrt{\frac{p_{atm} + \frac{2\sigma}{r}}{\rho_l + C}} \quad (4)$$

in which: χ means the coefficient of temperature conductivity.

For the micro-texture with a circular cross section, its hydraulic radius R equals $2r$; while for the real micro-texture with a cross section of equilateral triangle (side length a), its hydraulic radius R equals $\frac{\sqrt{3}a}{12}$. The initial penetration velocity

for micro-textures with a triangular cross section can be acquired by replacing the hydraulic radius in Eq. (4):

$$v_l = \sqrt{\frac{p_{atm} + \frac{48\sigma}{\sqrt{3}a}}{\rho_l + C}} \quad (5)$$

It can be seen from Eq. (5) that for a particular lubricant, the initial penetration velocity increases as the side length of the micro-texture's cross section decreases. This means that micro-textures with smaller size would benefit for the penetration of lubricant into the micro-texture, and thus into the cutting area, at the beginning of the penetration.

3 FEA analysis

3.1 FEA analysis setup

FEA analysis software COMSOL is used in this study. The illustration of the FEA analysis setup and the meshed model

Fig. 2 FEA analysis setup
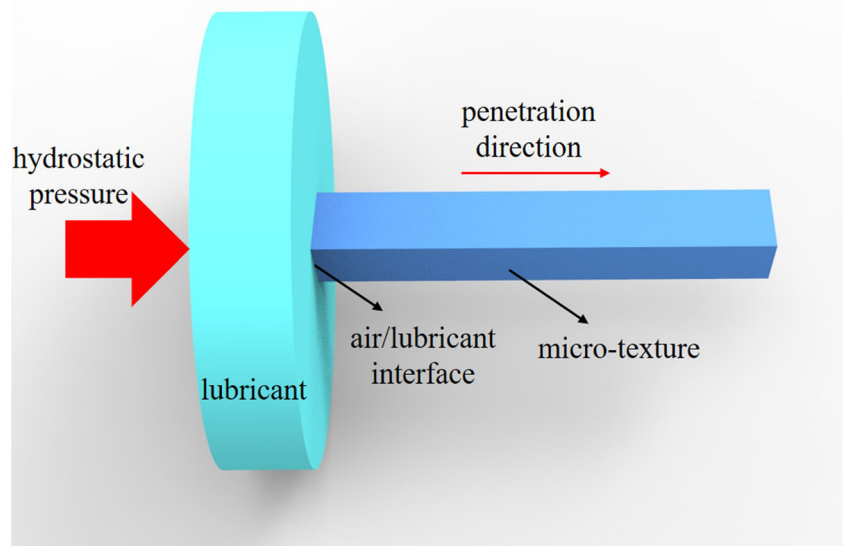
are exhibited in Fig. 2. This simulation model is consistent with the experimental setup and the flooded lubricant conditions during machining process. The FEA analysis model consists of the reservoir filled with lubricant and the micro-texture with a triangular cross section. The reservoir has a much larger size compared with the micro-texture, which would supply enough lubricant during FEA analysis process. Concerning the widely usage of water-based lubricant and green machining [29, 30] demands, the lubricant is set as water in this research, and the micro-texture is full of air before the FEA analysis. The lubricant penetrates the micro-texture because of wall adhesion and surface tension at the air/lubricant interface. To model the adhesive forces at the walls correctly, the treatment of the boundary conditions is important. A non-zero slip velocity and a frictional force at the wall are introduced. With such a boundary condition, it is possible to explicitly set the contact angle, that is, the angle between the fluid interface and the wall. Under such boundary setup, the pressure field, the velocity field, and the lubricant surface's shape and position can be calculated. The side length of the micro-texture's cross section is set from 20 to 180 μm with an interval of 40 μm.

Figure 3 shows the meshed model. The meshing process is done automatically through a physics-controlled mesh sequence type. Fine element size is used and a total of more than 80,000 tetrahedral elements is obtained. A transient solver is
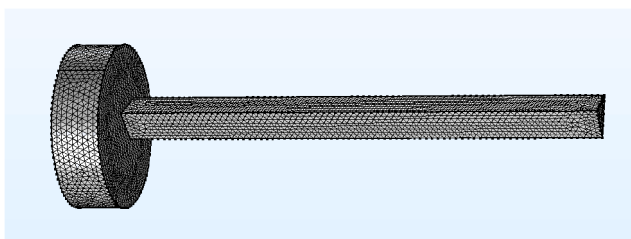
used. A convergence test is conducted prior the FEA analysis. Result shows that the solution is mesh independent, so the mesh density is sufficient. The penetration time is set as 0.001 s according to prior trials to ensure a reasonable penetration distance and a relatively short FEA analysis time.

3.2 FEA analysis results

Figure 4 illustrates the air/lubricant interface position at different penetration time. And obviously, the gradient of the tangent line at certain point for each curve stands for the penetration velocity at that point. It can be seen in Fig. 4 that at the beginning of the penetration, the penetration velocity for micro-texture with smaller size (e.g., 20 μm) is higher than that with larger size (e.g., 180 μm). This is in in accordance with the theory calculation above. However, when the penetration distance is larger than 0.15 mm, the penetration
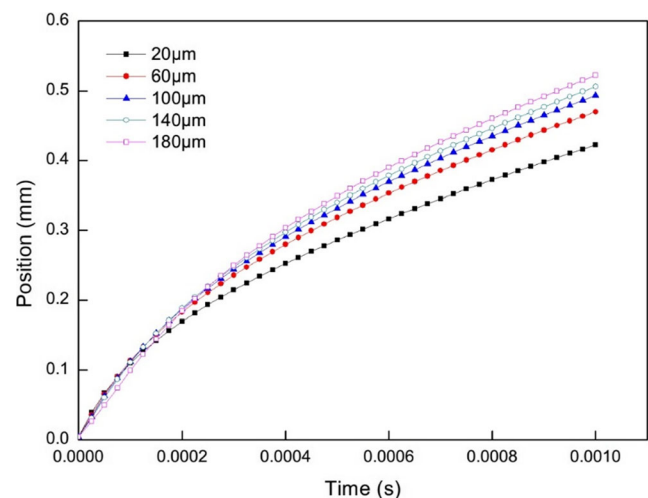

Fig. 3 Meshed model

Fig. 4 Air/lubricant interface position at different penetration time

velocity becomes larger for micro-texture with larger size gradually. And the penetration distance is much longer for micro-texture with larger size than that with smaller size at the same penetration time. At the end of the penetration time of 0.001 s, the penetration distance is longest for micro-texture with the largest side length of 180 μm.

4 Experiment analysis

4.1 Laser surface texturing

A prototype pulsed fiber laser (IPG, No: YLP-1-100-20-20-CN, Germany) machine is used as the fabrication laser in this study. The length of the micro-textures is set as 5 mm in this experimental study. After laser texturing, the specimen is carefully polished using sandpapers (1000#) to remove any bulges around the microgrooves and ultrasonically cleaned in fresh dehydrated alcohol. Subsequently, the width and depth of the microgrooves is measured by a stereo optical microscope (VHX-2000, Keyence Co., Japan). Finally, the hydraulic radius of the micro-textures is calculated.

4.2 Lubricant penetration experiment

Figure 5(a) shows the schematic of experimental setup for lubricant penetration experiment. A water channel is fabricated in advance at one end of the micro-textures to ensure that the lubricant starts to penetrate all the micro-textures at the same time. Water is used in this study as the lubricant in accordance with the simulation analysis and it is applied to the water channel using a dropper. Then the penetration of the lubricant in the micro-textures is recorded by the stereo optical microscope. The total time of the lubricant penetrating to the other end of the micro-textures is also recorded. The situ experimental setup is displayed in Fig. 5(b).

4.3 Experiment results

The morphology of the micro-textures fabricated using laser surface texturing is shown in Fig. 6. Particularly, the surface profiles at the red rectangle in Fig. 6(a) analyzed by the stereo optical microscope are shown in Fig. 6(b). It can be seen that different width of micro-textures can be obtained using laser surface texturing and the cross section of the microgrooves is in V-shape, which is in accordance with the FEA analysis. The micro-textures are marked as #1 to #6 from the top to the bottom in Fig. 6(a). The width of the micro-textures varies from 171.48 to 122.00 μm. The depth of the micro-textures is measured through the 3D profile of the micro-texture obtained by the stereo optical microscope. The width and depth of the micro-textures is
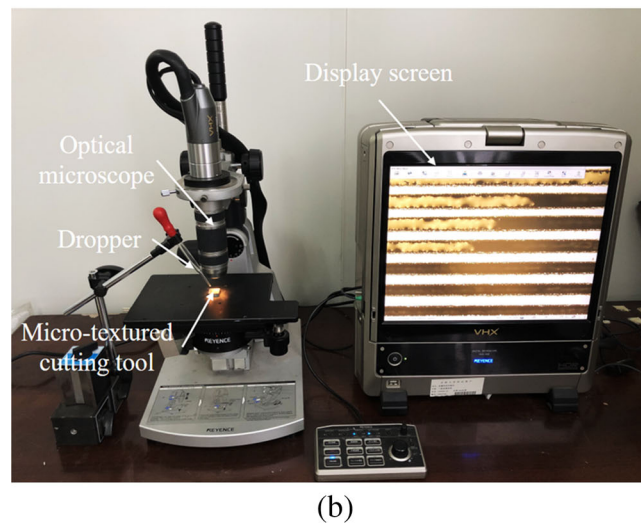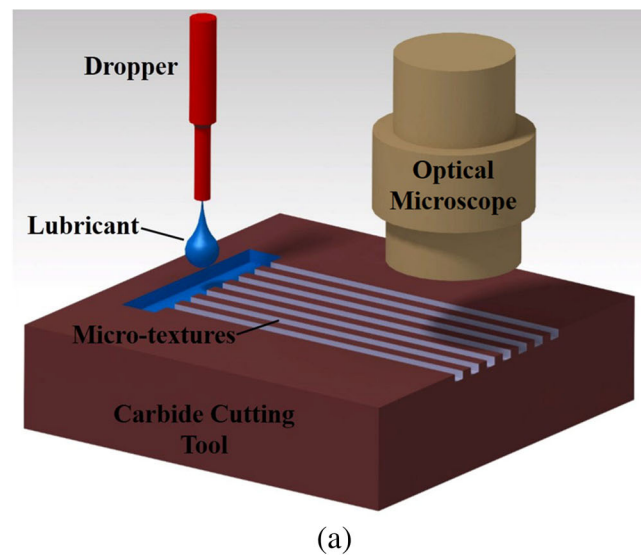

(a)

(b)

Fig. 5 **a** Schematic of experimental setup for lubricant penetration, **b** Situ experimental setup

summarized in Fig. 6. The hydraulic radius of the micro-textures is also calculated and depicted in Fig. 7.

The penetration process of the lubricant into the micro-textures recorded by the stereo optical microscope is shown in Fig. 8. It is quite clear in Fig. 8(a) that after a 3-s penetration, the lubricant penetrates to the middle of the optical microscope's shooting range in micro-texture #1, but there is no lubricant observed in micro-texture #3/4/5/6 at the same time. At the time of 4.5 s, the lubricant penetrates to the middle of the optical microscope's shooting range in micro-texture #6, while the lubricant already penetrates to the end of micro-texture #1/2/3/4.

5 Discussions

From the descriptions above, it can be seen that the results of theory calculation, FEA analysis and experiments match well

Fig. 6 Optical migrographs of the micro-textures. **a** Width of the micro-textures. **b** Surface profile of micro-texture #1

(a) Width of the micro-textures (b) Surface profile of micro-texture #1
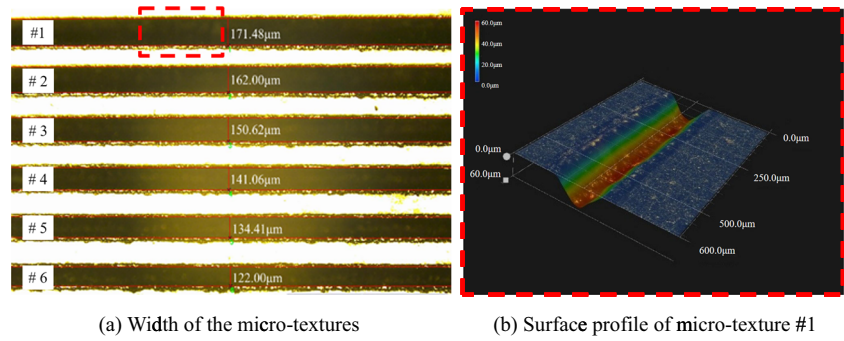
in this study. The initial penetration velocity of lubricant is higher when the cross section of the micro-texture is smaller. However, when the length of micro-texture is above 0.15 mm, the penetration distance of lubricant is longer for micro-textures with bigger cross section at the same penetration time.

The penetration of lubricant into the micro-texture is mainly driven by capillary action, which is the ability of a liquid flowing in narrow spaces without the assistance of external forces. The Young–Laplace equation is the description of the capillary pressure driven the lubricant penetrating into the micro-texture, and the most commonly used variation of equation is:

$$p_c = \frac{2\gamma\cos\theta}{r} \qquad (6)$$

where:

γ is the interfacial tension;
r is the effective radius of the interface, which is the hydraulic diameters in this study;
θ is the wetting angle of the liquid on the surface of the capillary.

It can be aware that smaller hydraulic diameter r leads to higher capillary pressure at the air/lubricant interface, and in turn the higher initial penetration velocity.
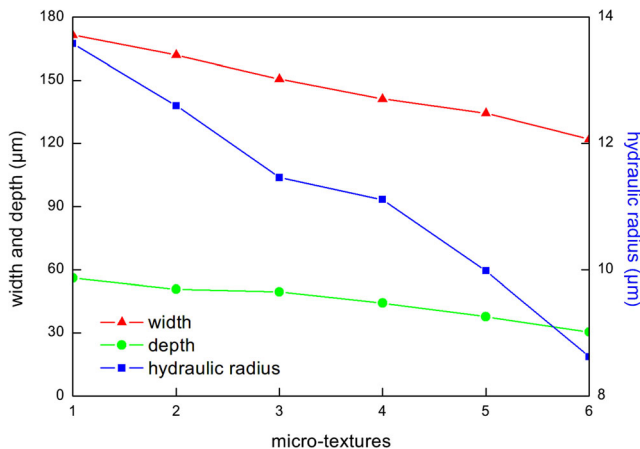

Fig. 7 Parameters of the micro-textures

As the lubricant penetrating into the micro-texture, friction force between the lubricant and the wall of the micro-texture would impede the flowing of the lubricant. Surely, the effect of the friction force is in relation with the ratio i of the perimeter to the area of the cross section of the micro-texture. For an equilateral triangle:

$$
\begin{aligned}
S &= 3a \\
A &= \frac{\sqrt{3}a^2}{4} \\
i &= \frac{S}{A} = \frac{4\sqrt{3}}{a}
\end{aligned}
\qquad (7)
$$

where:

S is the perimeter of the cross section of the micro-texture;
A is the area of the cross section of the micro-texture;
i is the ratio of the perimeter to the area of the cross section of the micro-texture.

It can be seen that the smaller the side length of the triangular, the bigger the ratio of the perimeter to the area of the cross section of the micro-texture, and in turn higher friction force per unit area. The combined action of the capillary pressure and the friction force results in the different results for lubricant penetration distance into the micro-texture.

Furthermore, the lubricant is applied to the water channel and in turn the micro-texture through a dropper during the lubricant penetration experiment. Hence, the initial penetration velocity of the lubricant is the composition of the velocity originated by the capillary pressure and the velocity introduced by the gravity during the dropping of the lubricant from the dropper to the water channel. This would reduce the advantages of higher initial penetration velocity due to the capillary action for micro-texture with smaller size.

In conclusion, if the back engagement is very small during cutting process, which means that the width of the chip is very small and the penetration distance for the lubricant is very small, smaller micro-texture should be introduced into the rake face of the cutting tool to facilitate the penetration of lubricant into the cutting area, as smaller size leads to higher initial penetration velocity. However, if the width of the cutting chip exceeds a certain value (about 0.15 mm under the

Fig. 8 Penetration process of the lubricant. **a** Time 3 s. **b** Time 3.5 s. **c** Time 4 s. d Time 4.5 s

(a) time: 3s

(b) time: 3.5s

(c) time: 4s

(d) time: 4.5s
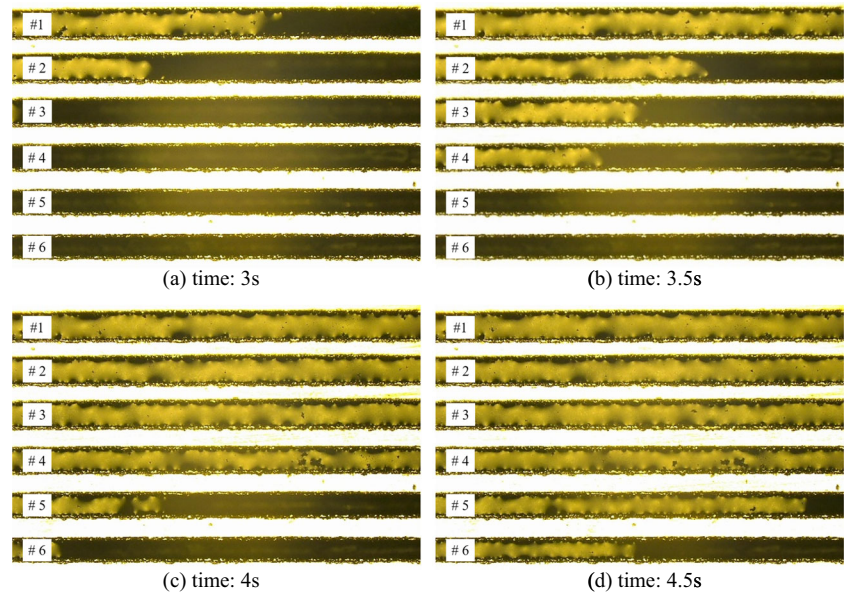
conditions in this study), the size of the micro-texture should be as big as possible. However, bigger micro-texture would have larger effect on the strength of the cutting tool. Thus, a reasonable size of the micro-texture should be chosen.

6 Conclusions

The penetration process of lubricant into micro-textures introduced into the rake face of the cutting tool during machining process is analyzed through theory calculation, FEA analysis and penetration experiments. The initial penetration velocity and penetration distance at the same time for micro-textures with different size are discussed. Several conclusions can be made:

(1) The initial penetration velocity increases as the side length of the micro-texture's cross section decreases.

(2) When the penetration distance is larger than 0.15 mm, penetration velocity for micro-texture with larger cross section size exceeds that for micro-texture with smaller size gradually.

(3) Micro-texture with smaller size is suitable for smaller chip width, 0.15 mm under the conditions in this study. And micro-texture with a larger size is suitable for large back engagement in consideration of lubricant penetration.

(4) An optimum size of micro-texture on the rake face of cutting tools should take both lubricant penetration and strength of the cutting tool into consideration.

References

1. Laperriere L (2014) CIRP encyclopedia of production engineering. Springer, Berlin
2. Özel T, Altan T (2000) Determination of workpiece flow stress and friction at the chip–tool contact for high-speed cutting. Int J Mach Tool Manu 40(1):133–152
3. Qi BY, Li L (2012) Experimental study on orthogonal cutting of Ti6Al4V with surface micro-groove textured cutting tool. Mater Sci Forum 723:243–246
4. Postnikov S (1967) Penetrating ability of cutting fluids. Wear 10(2): 142–150
5. Godlevski VA, Volkov AV, Latyshev VN et al (1998) A description of the lubricating action of the tribo-active components of cutting fluids. Lubr Sci 11(1):51–62
6. Zhang KD, Deng JX, Xing YQ, Li SP, Gao HH (2015) Effect of microscale texture on cutting performance of WC/Co-based TiAlN coated tools under different lubrication conditions. Appl Surf Sci 326:107–118
7. Trent EM (1988) Metal cutting and the tribology of seizure: I seizure in metal cutting. Wear 128(1):29–45
8. Enomoto T, Watanabe T, Aoki Y, Ohtake N (2007) Development of a cutting tool with micro structured surface. Trans Jpn Soc Mech Eng C 73(729):1560–1565
9. Li Q, Yang SC, Zhang YH, Zhou YZ, Cui JT (2018) Evaluation of the machinability of titanium alloy using a micro-textured ball end milling cutter. Int J Adv Manuf Technol 98(5-8):2083–2092
10. Sun JL, Zhou YH, Deng JX, Zhao J (2016) Effect of hybrid texture combining micro-pits and micro-grooves on cutting performance of WC/Co-based tools. Int J Adv Manuf Technol 86(9-12):3383–3394
11. Wang ZW, Chen MW, Wu JW, Zheng HH, Zheng XF (2010) A review of surface texture of tribological interfaces. Appl Mech Mater 37-38:41–45
12. Lei S, Devarajan S, Chang Z (2009) A study of micropool lubricated cutting tool in machining of mild steel. J Mater Process Technol 209(3):1612–1620
13. Duan R, Deng JX, Ai X, Liu YJ, Chen H (2017) Experimental assessment of derivative cutting of micro-textured tools in dry cutting of medium carbon steels. Int J Adv Manuf Technol 92(9-12): 3531–3540

14. Kim DM, Bajpai V, Kim BH, Park HW (2015) Finite element modeling of hard turning process via a micro-textured tool. Int J Adv Manuf Technol 78(9-12):1393–1405

15. Ma JF, Ge XC, Qiu CQ, Lei ST (2016) FEM assessment of performance of microhole textured cutting tool in dry machining of Ti-6Al-4V. Int J Adv Manuf Technol 84(9-12):2609–2621

16. Vasumathy D, Meena A, Duraiselvam M (2017) Experimental study on evaluating the effect of micro textured tools in turning AISI 316 austenitic stainless steel. Procedia Eng 184:50–57

17. Sugihara T, Nishimoto Y, Enomoto T (2017) Development of a novel cubic boron nitride cutting tool with a textured flank face for high-speed machining of Inconel 718. Precis Eng 48:75–82

18. Fatima A, Mativenga PT (2015) A comparative study on cutting performance of rake-flank face structured cutting tool in orthogonal cutting of AISI/SAE 4140. Int J Adv Manuf Technol 78(9-12):2097–2106

19. Sharma V, Pandey PM (2016) Geometrical design optimization of hybrid textured self-lubricating cutting inserts for turning 4340 hardened steel. Int J Adv Manuf Technol 89(5-8):1–15

20. Li Y, Deng JX, Chai YS, Fan WL (2016) Surface textures on cemented carbide cutting tools by micro EDM assisted with high-frequency vibration. Int J Adv Manuf Technol 82(9-12):2157–2165

21. Pang MH, Nie YF, Ma LJ (2018) Effect of symmetrical conical micro-grooved texture on tool–chip friction property of WC-TiC/Co cemented carbide tools. Int J Adv Manuf Technol 99(1-4):737–746

22. Ma JF, Duong NH, Lei ST (2015) 3D numerical investigation of the performance of microgroove textured cutting tool in dry machining of Ti-6Al-4V. Int J Adv Manuf Technol 79(5-8):1313–1323

23. Yin SB, Ji W, He GH, Liu XL, Wang LH (2018) Experimental evaluation on texture of flank face on tool wear in chamfer milling of stainless steel. Int J Adv Manuf Technol 99(9-12):2929–2937

24. Tang W, Zhou Y, Zhu H, Yang HF (2013) The effect of surface texturing on reducing the friction and wear of steel under lubricated sliding contact. Appl Surf Sci 273:199–204

25. Fang Z, Obikawa T (2017) Cooling performance of micro-texture at the tool flank face under high pressure jet coolant assistance. Precis Eng 49:41–51

26. Durairaj S, Guo J, Aramcharoen A, Castagne S (2018) An experimental study into the effect of micro-textures on the performance of cutting tool. Int J Adv Manuf Technol 98(1-4):1011–1030

27. Fatima A, Mativenga PT (2017) On the comparative cutting performance of nature-inspired structured cutting tool in dry cutting of AISI/SAE 4140. Proc Inst Mech Eng B-J Eng 231(11):1941–1948

28. Godlevski VA, Volkov AV, Latyshev VN, Maurin LN (1997) The kinetics of lubricant penetration action during machining. Lubr Sci 9(2):127–140

29. Kovacevic R, Cherukuthota C, Mazurkiewicz M (1995) High pressure waterjet cooling/lubrication to improve machining efficiency in milling. Int J Mach Tool Manu 35(10):1459–1473

30. Liu JY, Han RD, Wang Y (2010) Research on difficult-cut-material in cutting with application of water vapor as coolant and lubricant. Ind Lubr Tribol 62(5):251–262